A Detumbling Strategy for an Orbital Manipulator in the Post-Grasp Phase

Ria Vijayan, Marco De Stefano and Christian Ott

Abstract— **In this paper, we propose a detumbling strategy that stabilizes the motion of a tumbling client satellite using an orbital servicing manipulator, which is the goal of the post-grasp phase. One of the critical aspects in this phase is ensuring that excessive contact forces are not generated at the grasp interface. In addition, space mission requirements might demand a nominal manipulator configuration that is suitable for further manipulation/servicing activities.**

The proposed strategy allows the detumbling of the client motion while ensuring that the contact forces developed at the grasp interface do not violate a safety threshold. Further, it allows the reconfiguration of the manipulator arm by exploiting the full actuation capability of the manipulator-equipped servicing spacecraft. The controller guarantees joint task convergence in the nullspace of the manipulator's end-effector, and is also valid for kinematically singular configurations of the manipulator. It is further augmented using a quadratic programming based approach to optimally constrain the contact forces. Finally, simulation results for a post-grasp detumbling scenario are shown to validate the effectiveness of the proposed method.

I. INTRODUCTION

In an on-orbit servicing mission, a spacecraft equipped with a manipulator arm on its base (servicer) approaches and grasps a second satellite, the client (see Fig. 1). After the capture, the so-called post-grasp phase occurs, where the goal of the servicer is to detumble the system, i.e. to stabilize the combined motion. Later, servicing tasks such as refuelling and maintenance can be executed using the manipulator arm [1]. In recent on-orbit servicing mission studies (see e.g. the DEOS mission [2], the COMRADE or the e.Deorbit project [3], [4]), the client is considered to be a free-tumbling and non-cooperative satellite, which means that the support from the attitude and orbit control of the client satellite is not available. This factor poses a challenge for the control design, which further needs to respect the force limits of the grasping interface to avoid damage, and consequently, loss of the client [5].

The coordinated control of the manipulator and spacecraft provides great flexibility to orbital servicing [6], [7]. In [8], control for a multi-arm orbital manipulator is developed for the approach and capture phases. A momentum dumping strategy is presented in [9] using external actuation to remove the accumulated momentum from contacts occurring during the capture phase. In [10], a shared control strategy between teleoperation and autonomous control was proposed, to achieve a primary task on the end-effector, and a secondary task on the base. The problem of actuating the base and manipulator at different frequencies is addressed in [11].

All the authors are with the Institute of Robotics and Mechatronics, German Aerospace Center (DLR), 82234 Wessling, Germany. Contact: ria.vijayan@dlr.de

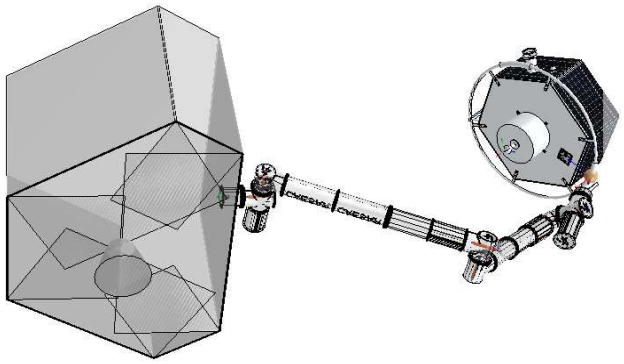

Fig. 1: Left: servicer satellite equipped with a manipulator arm (CAESAR arm [18]). Right: captured client satellite.

The capture strategies for the grasping phase have been approached from different perspectives. The concept of virtual-mass for impedance matching control was introduced in [12] to determine that, the contact between the end-effector and client is maintained, if the impedance at the end-effector is equal to (or smaller) than the client's mass. The center of percussion of a space robot is analyzed in [13] to formulate guidelines for impact minimization while capturing a client. A disturbance observer is implemented in [14] to estimate the contact forces during impact, which is then compensated in an impedance controller to achieve compliant capture.

Post-grasp momentum stabilization approaches that lead to minimum disturbance in the attitude of the base, have been proposed in the past. In [15], a strategy to transfer the impact momentum from the base to the manipulator is proposed, while simultaneously damping the joint velocities through the reaction null space [16]. In [17], the distribution of angular momentum of the client between the base, reaction wheels and manipulator, while utilizing the reaction null space, was demonstrated.

A common approach for stabilizing the motion of a spinning satellite is to design a suitable detumbling trajectory. In [19], a time-optimal detumbling trajectory that limits the interaction torque during the grasping, is tracked by a feedback linearized control, while the base's attitude control system compensates the transferred angular momentum. This approach is further extended in [20] to energy-optimal trajectories. Similarly, a time-optimal maneuver is presented in [5] to detumble along an arbitrary motion of the manipulator while constraining the measurable contact forces. An energy-optimal approach for joint tracking control, to rigidize the arm in the post-grasp stabilization, was proposed in [21]. A

direct force controller to respect the contact force limits while detumbling the target is presented in [22]. A hybrid motion and force control is developed in [23] while detumbling the target along polynomial trajectories. An impedance controller was designed in [24] to damp the motion of a tumbling target by assuming the internal contact forces at the grasp as external forces acting on the end-effector.

In this paper, we focus on post-grasp motion stabilization, i.e. detumbling, while satisfying constraints on grasping contact forces and requirements on manipulator configuration. In contrast with [15], [16], [17], we relax the restriction on the attitude of the base in the post-grasp phase, and prioritize the manipulator reconfiguration (which may be required for a detumbling strategy, see e.g. [21]). This is achieved by exploiting the motion of the base. Further, in contrast with [5], [20], [21], we do not consider an optimal detumbling trajectory for the client, and unlike [5], [12], [22], we also does not rely on force/torque measurements. The proposed controller detumbles the system using a fully-actuated servicer, while respecting contact force limits imposed by space mission requirements in the post-grasp phase.

The contributions of this paper are twofold. First, a novel control strategy for the post-grasp motion stabilization of a free-tumbling client is developed. The controller achieves the detumbling of the client satellite and the reconfiguration of the manipulator arm to a desired joint pose. To this end, we exploit the nullspace of the servicer's end-effector using the full actuation of the servicer. The proposed controller is shown to be valid also for kinematically singular configurations of the manipulator. Second, the controller is extended using a quadratic programming (QP) approach to constrain the contact forces developed in the post-grasp phase in an optimal manner and it does not require force feedback. Simulation results validate the proposed method.

The structure of the paper is as follows. Sec. II describes the dynamic model of the system in the post-grasp phase. Sec. III introduces the controller design for the proposed detumbling strategy. Sec. IV presents the QP approach to limit the contact forces. Sec. V illustrates the results from a dynamic simulation, and Sec. VI concludes the work.

II. Post-Grasp Dynamic Modeling

In this section, preliminaries on the modeling of the whole system are described. The system is composed of a fully-actuated orbital manipulator called the *servicer*, i.e. a base spacecraft equipped with a manipulator arm, and the *client*, i.e. the non-cooperative satellite that has been captured. The post-grasp dynamics is modeled with the standard approach used in robotic grasp dynamics [25]. The dynamics of the servicer and client are as follows,

$$\boldsymbol{M_s}\dot{\boldsymbol{\nu}}_{\boldsymbol{s}}+\boldsymbol{C_s}\boldsymbol{\nu_s}=\boldsymbol{\Gamma}+\boldsymbol{J}^T\boldsymbol{F_c}, \tag{1}$$

$$\boldsymbol{M_c}\dot{\boldsymbol{\nu}}_{\boldsymbol{c}}+\boldsymbol{C_c}\boldsymbol{\nu_c}=-\boldsymbol{J_c}^T\boldsymbol{F_c}, \tag{2}$$

where $\boldsymbol{M_s},\boldsymbol{C_s}\in\mathbb{R}^{6+n\times 6+n}$ and $\boldsymbol{M_c},\boldsymbol{C_c}\in\mathbb{R}^{6\times 6}$, are the inertia and Coriolis matrices of the servicer and client dynamics respectively and n represents the number of Degrees of Freedom (DoF) of the manipulator. The servicer's state is given by $\boldsymbol{\nu_s}=\begin{bmatrix}\boldsymbol{\nu_b}^T & \dot{\boldsymbol{q}}^T\end{bmatrix}^T\in\mathbb{R}^{6+n}$ where $\boldsymbol{\nu_b}\in\mathbb{R}^6$, is the Cartesian velocity (linear and angular) of the base in body frame and $\dot{\boldsymbol{q}}\in\mathbb{R}^n$, are the joint rates. The state $\boldsymbol{\nu_c}\in\mathbb{R}^6$, is the Cartesian velocity of the client in body frame. The actuation on the servicer, $\boldsymbol{\Gamma}=\begin{bmatrix}\boldsymbol{F_b}^T & \boldsymbol{\tau}^T\end{bmatrix}^T\in\mathbb{R}^{6+n}$, includes $\boldsymbol{F_b}\in\mathbb{R}^6$, the wrench input to the base in body frame, and $\boldsymbol{\tau}\in\mathbb{R}^n$, the joint torques applied on the manipulator. The servicer's Jacobian matrix, $\boldsymbol{J}=\begin{bmatrix}\boldsymbol{J_b} & \boldsymbol{J_m}\end{bmatrix}\in\mathbb{R}^{6\times 6+n}$, maps $\boldsymbol{\nu_s}$ to $\boldsymbol{\nu_e}\in\mathbb{R}^6$, the end-effector Cartesian velocity. $\boldsymbol{J_b}\in\mathbb{R}^{6\times 6},\boldsymbol{J_m}\in\mathbb{R}^{6\times n}$, are the base and manipulator Jacobians respectively. Note that $\boldsymbol{J_b}$ is an adjoint transformation and thus invertible. Therefore, $\boldsymbol{J}$ always has full row rank independent of the kinematic singularities of the manipulator. $\boldsymbol{J_c}\in\mathbb{R}^{6\times 6}$ is the client's Jacobian matrix mapping $\boldsymbol{\nu_c}$ to the Cartesian velocity at the grasping point. Lastly, $\boldsymbol{F_c}\in\mathbb{R}^6$ is the contact wrench acting between the manipulator's end-effector and the client's grasping point expressed in the end-effector frame.

Further, considering a rigid grasp, the combined system is subjected to the velocity constraint at the grasping point,

$$\boldsymbol{\nu_e}=\boldsymbol{J}\boldsymbol{\nu_s}=\boldsymbol{J_c}\boldsymbol{\nu_c}. \tag{3}$$

Here, $\boldsymbol{J_c}$ is an invertible adjoint transformation. Hence, using the constraint in (3), $\boldsymbol{\nu_c}$ and it's time-derivative can be substituted in (2). In the post-grasp phase, the contact forces, $\boldsymbol{F_c}$, are considered as internal forces acting on the system at the grasping point. Therefore (1) and (2) can be combined to obtain the post-grasp dynamics as follows [19],

$$\boldsymbol{M}\dot{\boldsymbol{\nu}}_{\boldsymbol{s}}+\boldsymbol{C}\boldsymbol{\nu_s}=\boldsymbol{\Gamma}, \tag{4}$$

where,

$$\begin{aligned}\boldsymbol{M}&=\boldsymbol{M_s}+\boldsymbol{J}^T\boldsymbol{J_c}^{-T}\boldsymbol{M_c}\boldsymbol{J_c}^{-1}\boldsymbol{J},\\ \boldsymbol{C}&=\boldsymbol{C_s}+\boldsymbol{J}^T\boldsymbol{J_c}^{-T}\boldsymbol{C_c}\boldsymbol{J_c}^{-1}\boldsymbol{J}+\boldsymbol{J}^T\boldsymbol{J_c}^{-T}\boldsymbol{M_c}\frac{d}{dt}(\boldsymbol{J_c}^{-1}\boldsymbol{J}).\end{aligned} \tag{5}$$

The post-grasp model in (4) will be used for the controller design, where we assume that the inertia parameters of the client are known (as considered in e.g. [19]).

III. Controller Design

The goal of the controller is to stabilize the motion of the servicer-client system while reconfiguring the manipulator arm. The strategy adopted considers a Cartesian damping control acting on the end-effector, while nullspace control is used to reconfigure the joints and damp the motion of the base. To this end, the end-effector velocity, $\boldsymbol{\nu_e}$, is augmented by the nullspace velocity, $\boldsymbol{\nu_n}\in\mathbb{R}^n$, such that the extended Jacobian, $\boldsymbol{J_N}$, is invertible (see [26] for details),

$$\begin{bmatrix}\boldsymbol{\nu_e}\\ \boldsymbol{\nu_n}\end{bmatrix}=\boldsymbol{J_N}\boldsymbol{\nu_s},\quad \boldsymbol{J_N}=\begin{bmatrix}\boldsymbol{J}\\ \boldsymbol{N}\end{bmatrix}, \tag{6}$$

where,

$$\boldsymbol{N}=(\boldsymbol{Z}\boldsymbol{M}\boldsymbol{Z}^T)^{-1}\boldsymbol{Z}\boldsymbol{M},\quad \boldsymbol{Z}=\begin{bmatrix}-\boldsymbol{J_m}^T\mathrm{adj}(\boldsymbol{J_b})^T & \det(\boldsymbol{J_b})\boldsymbol{I}\end{bmatrix}. \tag{7}$$

$\boldsymbol{Z}\in\mathbb{R}^{n\times 6+n}$ is a basis matrix for the nullspace of $\boldsymbol{J}$ such that the property $\boldsymbol{Z}\boldsymbol{J}^T=\boldsymbol{0}$ is satisfied [27], and $\boldsymbol{I}\in\mathbb{R}^{n\times n}$ is an identity matrix. Hence the nullspace is n-dimensional since $\det(\boldsymbol{J_b})=1$ as $\boldsymbol{J_b}$ is an invertible adjoint transformation.

Notice that, substituting $\boldsymbol{M}$ from (5) into $\boldsymbol{N}$ in (7) implies,

$$\begin{aligned} \boldsymbol{ZM} &= \boldsymbol{ZM_s} + \boldsymbol{ZJ}^T \boldsymbol{J_c}^{-T} \boldsymbol{M_c} \boldsymbol{J_c}^{-1} \boldsymbol{J}, \\ \Rightarrow \boldsymbol{N} &= (\boldsymbol{ZM_s Z}^T)^{-1} \boldsymbol{ZM_s}, \end{aligned} \tag{8}$$

where the relation between the servicer's Jacobian and its nullspace, $\boldsymbol{ZJ}^T = \boldsymbol{0}$ is used. Therefore, the inertia parameters of the client do not affect the nullspace velocities.

To facilitate the design of the controller, (4) is transformed to the augmented task velocity coordinates as,

$$\underbrace{\begin{bmatrix} \boldsymbol{\Lambda_e} & \boldsymbol{0} \\ \boldsymbol{0} & \boldsymbol{\Lambda_n} \end{bmatrix}}_{\boldsymbol{\Lambda}} \begin{bmatrix} \dot{\boldsymbol{v}}_e \\ \dot{\boldsymbol{v}}_n \end{bmatrix} + \underbrace{\begin{bmatrix} \boldsymbol{\mu_{ee}} & \boldsymbol{\mu_{en}} \\ \boldsymbol{\mu_{ne}} & \boldsymbol{\mu_{nn}} \end{bmatrix}}_{\boldsymbol{\mu}} \begin{bmatrix} \boldsymbol{v_e} \\ \boldsymbol{v_n} \end{bmatrix} = \underbrace{\begin{bmatrix} \boldsymbol{F_e} \\ \boldsymbol{F_n} \end{bmatrix}}_{\boldsymbol{F}}, \tag{9}$$

where,

$$\begin{aligned} &\boldsymbol{\Lambda} = \boldsymbol{J_N}^{-T} \boldsymbol{M} \boldsymbol{J_N}^{-1}, \qquad \boldsymbol{\mu} = \boldsymbol{J_N}^{-T} \boldsymbol{M} \frac{d}{dt}(\boldsymbol{J_N}^{-1}) + \boldsymbol{J_N}^{-T} \boldsymbol{C} \boldsymbol{J_N}^{-1}, \\ &\boldsymbol{J_N}^{-1} = \begin{bmatrix} \boldsymbol{J}^{\boldsymbol{M}+} & \boldsymbol{Z}^T \end{bmatrix}, \quad \boldsymbol{F} = \boldsymbol{J_N}^{-T} \boldsymbol{\Gamma}, \end{aligned} \tag{10}$$

and $\boldsymbol{J}^{\boldsymbol{M}+} = \boldsymbol{M}^{-1} \boldsymbol{J}^T (\boldsymbol{J} \boldsymbol{M}^{-1} \boldsymbol{J}^T)^{-1}$ is the dynamically consistent generalized inverse of $\boldsymbol{J}$ [28]. Since $\boldsymbol{N}$ in (8) was shown to be independent of the client's inertia parameters, consequently $\boldsymbol{J_N}^{-1}$ will also be independent of $\boldsymbol{M_c}$.

The controller is designed such that the Cartesian space control, $\boldsymbol{F_e}$, damps the end-effector velocity, thus stabilizing the client. Whereas, the null space control, $\boldsymbol{F_n}$, reconfigures the arm while stabilizing the base. Therefore, the control wrenches are chosen as follows,

$$\boldsymbol{F_e} = -\boldsymbol{K_{De}} \boldsymbol{v_e} + \boldsymbol{\mu_{en}} \boldsymbol{v_n}, \tag{11}$$

$$\boldsymbol{F_n} = \boldsymbol{Z} \begin{bmatrix} \boldsymbol{0} \\ \boldsymbol{K_{Pq}} \boldsymbol{\Delta q}, \end{bmatrix} - \boldsymbol{Z} \begin{bmatrix} \boldsymbol{K_{Db}} \boldsymbol{v_b} \\ \boldsymbol{K_{Dq}} \dot{\boldsymbol{q}}, \end{bmatrix}, \tag{12}$$

where $\boldsymbol{K_{De}}, \boldsymbol{K_{Db}} \in \mathbb{R}^{6\times 6}$ and $\boldsymbol{K_{Dq}} \in \mathbb{R}^{n\times n}$ are positive-definite damping gain matrices of the end-effector, servicer base and manipulator joints, respectively. $\boldsymbol{K_{Pq}} \in \mathbb{R}^{n\times n}$ is the positive-definite joint stiffness matrix. $\boldsymbol{\Delta q} = \boldsymbol{q^d} - \boldsymbol{q}$ is the error between the desired joint angles $\boldsymbol{q^d}$ and measured angles $\boldsymbol{q}$. Note that the last term in (11) compensates the Coriolis coupling in order to decouple the end-effector task from the nullspace dynamics.

The control input to the servicer in (4) is obtained using (10) that relates the control wrenches designed in (11)-(12) to Γ using the extended Jacobian-transpose $\boldsymbol{J_N}^T$, resulting in,

$$\boldsymbol{\Gamma} = \underbrace{\boldsymbol{J}^T \boldsymbol{F_{De}}}_{\boldsymbol{\Gamma_1}} + \underbrace{\boldsymbol{N}^T \boldsymbol{Z} \boldsymbol{\Gamma_0}}_{\boldsymbol{\Gamma_2}} + \underbrace{\boldsymbol{J}^T \boldsymbol{\mu_{en}} \boldsymbol{v_n}}_{\boldsymbol{\Gamma_3}} \tag{13}$$

where,

$$\begin{aligned} \boldsymbol{F_{De}} &= -\boldsymbol{K_{De}} \boldsymbol{v_e} & \boldsymbol{\Gamma_0} &= \begin{bmatrix} \boldsymbol{F_{Db}}^T & \boldsymbol{\tau_{PD}}^T \end{bmatrix}^T \\ \boldsymbol{F_{Db}} &= -\boldsymbol{K_{Db}} \boldsymbol{v_b} & \boldsymbol{\tau_{PD}} &= \boldsymbol{K_{Pq}} \boldsymbol{\Delta q} - \boldsymbol{K_{Dq}} \dot{\boldsymbol{q}}. \end{aligned}$$

Note that $\boldsymbol{\Gamma_0}$ is projected onto the nullspace of $\boldsymbol{J}^T$ through[1] $\boldsymbol{N}^T \boldsymbol{Z}$. To summarize, the controller in (13) is composed of three terms, namely $\boldsymbol{\Gamma_1}$, which damps the end-effector velocity, $\boldsymbol{\Gamma_2}$ for the reconfiguration of the manipulator in the nullspace, and $\boldsymbol{\Gamma_3}$ to decouple the end-effector from nullspace dynamics. We note that the terms $\boldsymbol{\Gamma_1}$ and $\boldsymbol{\Gamma_2}$ are completely independent of the client inertia parameters, whereas $\boldsymbol{\Gamma_3}$ has a dependency through the Coriolis coupling between the end-effector task and nullspace. The dependency on servicer's inertia parameters are seen only via the nullspace matrix[2] $\boldsymbol{N}$. A block diagram of the designed controller is shown in Fig. 2.

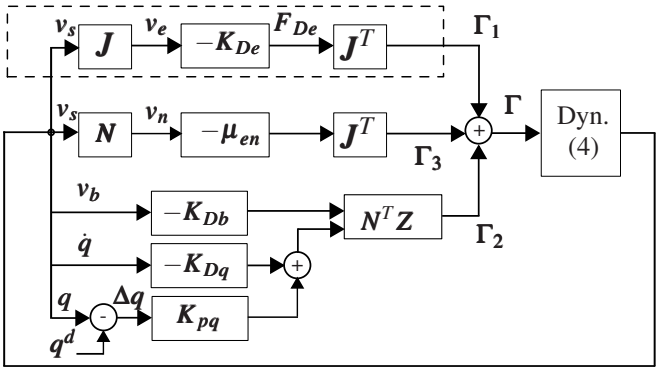

Fig. 2: Block diagram of the designed controller in closed-loop with the dynamics, used for the post-grasp phase.

1) Convergence of augmented task velocities: The controller designed in (13) can be analyzed similar to [26]. First, considering $V_e = \frac{1}{2} \boldsymbol{v_e}^T \boldsymbol{\Lambda_e} \boldsymbol{v_e}$ as the positive semi-definite Lyapunov function, and choosing $\boldsymbol{F_e}$ in (11), leads to

$$\dot{V}_e = \boldsymbol{v_e}^T \boldsymbol{F_{De}} = -\boldsymbol{v_e}^T \boldsymbol{K_{De}} \boldsymbol{v_e} \leq 0. \tag{14}$$

Second, considering $V_n = \frac{1}{2} \boldsymbol{v_n}^T \boldsymbol{\Lambda_n} \boldsymbol{v_n} + \frac{1}{2} \boldsymbol{\Delta q}^T \boldsymbol{K_{Pq}} \boldsymbol{\Delta q}$, and choosing $\boldsymbol{F_n}$ in (12), leads to

$$\dot{V}_n = -\boldsymbol{v_n}^T \boldsymbol{Z} \begin{bmatrix} \boldsymbol{K_{Db}} & \boldsymbol{0} \\ \boldsymbol{0} & \boldsymbol{K_{Dq}} \end{bmatrix} \boldsymbol{Z}^T \boldsymbol{v_n} \leq 0 \tag{15}$$

in the set where end-effector velocity, $\boldsymbol{v_e}$, goes to zero. The convergence of the augmented task velocities is seen from (14) and (15). A more detailed analysis on the stability of similar task space and nullspace control can be found in [30].

2) Convergence of joint task in the nullspace: It can be shown that, the joint errors converge to zero in the nullspace of the manipulator's end-effector for a fully-actuated base. This is unlike the nullspace control of an unactuated base with a redundant manipulator. The convergence in the case of the fully-actuated base is evident from the contribution of the stiffness term in (12), which vanishes only when,

$$\underbrace{\begin{bmatrix} -\boldsymbol{J_m}^T \text{adj}(\boldsymbol{J_b})^T & \det(\boldsymbol{J_b}) \boldsymbol{I} \end{bmatrix}}_{\boldsymbol{Z}} \begin{bmatrix} \boldsymbol{0} \\ \boldsymbol{K_{Pq}} \boldsymbol{\Delta q} \end{bmatrix} = \boldsymbol{0},$$

i.e. when $\boldsymbol{\Delta q} = \boldsymbol{0}$. This is due to $\det(\boldsymbol{J_b}) \boldsymbol{I}$ having rank n, leading to convergence of the joint task, as the nullspace and joint space have equal dimensions.

Alternatively, if in addition to the joint task, the base configuration is controlled in the nullspace, an additional stiffness would be added to the base (e.g. $\boldsymbol{K_{Pb}}$). However, this

[1]It is worth mentioning that $\boldsymbol{N}^T \boldsymbol{Z} = \boldsymbol{I} - \boldsymbol{J}^T \boldsymbol{J}^{\boldsymbol{M}+T}$, which is a common form of the nullspace projection matrix [28].

[2]The uncertainties in inertia parameters of the servicer can be expected to have minimal influence for a similar controller (see [29]).

could conflict with the joint task, which implicitly controls the base configuration relative to the client, and result in the controller converging to a local minimum of the potential, $V_{\boldsymbol{x_b},\boldsymbol{q}} = \frac{1}{2}\boldsymbol{\Delta x_b}^T \boldsymbol{K_{Pb}} \boldsymbol{\Delta x_b} + \frac{1}{2}\boldsymbol{\Delta q}^T \boldsymbol{K_{Pq}} \boldsymbol{\Delta q}$, where $\boldsymbol{\Delta x_b}$ is the error in position and orientation of the base. This occurs when,

$$\boldsymbol{Z}\begin{bmatrix}\boldsymbol{K_{Pb}}\boldsymbol{\Delta x_b}\\ \boldsymbol{K_{Pq}}\boldsymbol{\Delta q}\end{bmatrix} = \boldsymbol{0}, \quad \begin{bmatrix}\boldsymbol{\Delta x_b}\\ \boldsymbol{\Delta q}\end{bmatrix} \neq \boldsymbol{0}$$
$$\Rightarrow \boldsymbol{J_m}^T \mathrm{adj}(\boldsymbol{J_b})^T \boldsymbol{K_{Pb}} \boldsymbol{\Delta x_b} = \det(\boldsymbol{J_b}) \boldsymbol{K_{Pq}} \boldsymbol{\Delta q}.$$

In this scenario, the base and joint tasks cancel each other, reaching a displaced equilibrium, and reconfiguration of the arm in the nullspace is not guaranteed. However, since the controller designed in (13) does not include a task on the base, joint task convergence in the nullspace is achieved.

3) Validity of controller under kinematic singularities of the manipulator: The fully-actuated servicer is inherently redundant with respect to the end-effector Cartesian task due to 6-DoF actuation of the base in addition to joint actuation of the manipulator. Hence the degree of redundancy of the system is n in the presence of an n-DoF manipulator. This implies, the controller designed in (13) can also operate in kinematically singular configurations of the manipulator arm. This is seen from the nullspace matrix, $\boldsymbol{N}$, which exists for all configurations of the arm. As seen in (7), for $\boldsymbol{N}$ to exist, the rank of $\boldsymbol{Z}$ must be equal to n, which is true independent of the configuration of the arm. A physical intuition to this lies in the observation that the restriction on the directions of motion, imposed by the arm in a singular configuration, can be overcome by an appropriate motion of the base.

IV. Optimal QP-based control

The controller designed in Sec. III achieves the task of reconfiguring the arm while stabilizing the motion of the servicer and client, however, the contact forces of the grasp are not guaranteed to remain within a tolerable threshold. Respecting the contact force limits is a requirement in a space mission so as to avoid mechanical damage of the grasp interface and loss of client from the servicer's grasp [19].

A. Computation of the contact wrench

The contact wrench is the force and torque, which acts during the post-grasp phase between the servicer's end-effector and the client's grasping point. This is computed as a function of the control applied to the base and joints (see [25]) by using the velocity constraint in (3). In particular, by reformulating the velocity constraint as $\boldsymbol{A}\begin{bmatrix}\boldsymbol{v_s}^T & \boldsymbol{v_c}^T\end{bmatrix}^T = \boldsymbol{0}$, where $\boldsymbol{A} = \begin{bmatrix}-\boldsymbol{J} & \boldsymbol{J_c}\end{bmatrix}$, and taking its time-derivative combined with $\begin{bmatrix}\dot{\boldsymbol{v}}_s^T & \dot{\boldsymbol{v}}_c^T\end{bmatrix}^T$ from (1) and (2), the contact wrench is obtained as follows,

$$\boldsymbol{F_c} = \left(\boldsymbol{A}\boldsymbol{M_{sc}}^{-1}\boldsymbol{A}^T\right)^{-1}\left[\boldsymbol{A}\boldsymbol{M_{sc}}^{-1}\left(\begin{bmatrix}\boldsymbol{\Gamma}\\ \boldsymbol{0}\end{bmatrix} - \boldsymbol{C_{sc}}\begin{bmatrix}\boldsymbol{v_s}\\ \boldsymbol{v_c}\end{bmatrix}\right) + \dot{\boldsymbol{A}}\begin{bmatrix}\boldsymbol{v_s}\\ \boldsymbol{v_c}\end{bmatrix}\right], \tag{16}$$

where,

$$\boldsymbol{M_{sc}} = \begin{bmatrix}\boldsymbol{M_s} & \boldsymbol{0}\\ \boldsymbol{0} & \boldsymbol{M_c}\end{bmatrix} \qquad \boldsymbol{C_{sc}} = \begin{bmatrix}\boldsymbol{C_s} & \boldsymbol{0}\\ \boldsymbol{0} & \boldsymbol{C_c}\end{bmatrix}.$$

Note here the term $\boldsymbol{A}\boldsymbol{M_{sc}}^{-1}\boldsymbol{A}^T$ is invertible since $\boldsymbol{A}$ has full rank as both $\boldsymbol{J}$ and $\boldsymbol{J_c}$ have full rank, and the client velocity is computed from (3) as $\boldsymbol{v_c} = \boldsymbol{J_c}^{-1}\boldsymbol{J}\boldsymbol{v_s}$.

B. QP Optimization for the controller effort

In this section, we elaborate on a QP-based optimization of the controller presented in Sec. III. The main goal is to limit the contact wrench in (16) through the control effort in an optimal way, while preserving the structure of the controller designed in (13). In order to do this, we analyze the control variables in (13) to determine which variables to optimize.

First, to maintain the decoupling of the nullspace and the end-effector, the control effort, $\boldsymbol{\Gamma_3}$, shall be retained without modification. Next, the variable $\boldsymbol{\Gamma_2}$ in (13) could be modified by optimizing the variable $\boldsymbol{\Gamma_0}$ and projecting it into the nullspace. However, we first determine the contribution of the nullspace term $\boldsymbol{\Gamma_2}$ to the contact force by taking a closer look at (16). Analyzing the part of the expression in (16) that multiplies with $\boldsymbol{\Gamma_2}$ as follows,

$$\boldsymbol{A}\boldsymbol{M_{sc}}^{-1}\begin{bmatrix}\boldsymbol{\Gamma_2}\\ \boldsymbol{0}\end{bmatrix} = -\boldsymbol{J}\boldsymbol{M_s}^{-1}\boldsymbol{N}^T\boldsymbol{Z}\boldsymbol{\Gamma_0}$$

and substituting for $\boldsymbol{N}$ from (8), we obtain

$$\boldsymbol{J}\boldsymbol{Z}^T(\boldsymbol{Z}\boldsymbol{M_s}\boldsymbol{Z}^T)^{-1}\boldsymbol{Z}\boldsymbol{\Gamma_0} = \boldsymbol{0},$$

where the relation between the servicer's Jacobian and its nullspace, $\boldsymbol{J}\boldsymbol{Z}^T = \boldsymbol{0}$ is used. Hence, the nullspace control has no influence on the contact force $\boldsymbol{F_c}$. This is consistent with the knowledge that, the dynamically consistent nullspace projection does not directly produce a wrench at the end-effector. Therefore, we retain the control effort $\boldsymbol{\Gamma_2}$, which reconfigures the arm in the nullspace, without modification.

Lastly, the control effort $\boldsymbol{\Gamma_1}$, is primarily seen to be responsible for the contact wrench. In particular, $\boldsymbol{F_c}$ is largely a function of $\boldsymbol{F_{De}}$. This implies that $\boldsymbol{F_{De}}$ is the ideal candidate for optimization. In addition, optimizing $\boldsymbol{F_{De}}$ instead of $\boldsymbol{\Gamma_1}$ directly, maintains the Jacobian-transposed structure of the controller designed in (13). Although one could reduce $\boldsymbol{F_{De}}$, and thereby $\boldsymbol{F_c}$, by lowering the gain $\boldsymbol{K_{De}}$, this approach does not guarantee the contact forces limits as compared to a rigorous constrained-optimization of $\boldsymbol{F_{De}}$.

Therefore, the optimization of the proposed controller is formulated as the following QP problem,

$$\min_{\boldsymbol{F_{opt}}} \quad \frac{1}{2}(\boldsymbol{F_{opt}} - \boldsymbol{F_{De}})^T \boldsymbol{Q}(\boldsymbol{F_{opt}} - \boldsymbol{F_{De}}) \tag{17}$$
$$\text{s.t. } |\boldsymbol{F_c}|_i \leq \boldsymbol{F_{max_i}} \tag{18}$$
$$\boldsymbol{v_e}^T \boldsymbol{F_{opt}} \leq 0. \tag{19}$$

$\boldsymbol{Q} \in \mathbb{R}^{6\times 6}$ is a positive definite weighting matrix and $\boldsymbol{F_{opt}}$ is the optimized control wrench, which will modify $\boldsymbol{\Gamma_1}$ in (13) with $\boldsymbol{\Gamma_1^*} = \boldsymbol{J}^T\boldsymbol{F_{opt}}$. The chosen cost function minimizes the distance of the optimal wrench to the desired wrench $\boldsymbol{F_{De}}$.

In order to respect the contact force limits, dictated by space mission requirements, the constraint in (18) is added. This constraint ensures that the contact force $\boldsymbol{F_c}$, developed at the grasp point, does not exceed the component-wise, i,

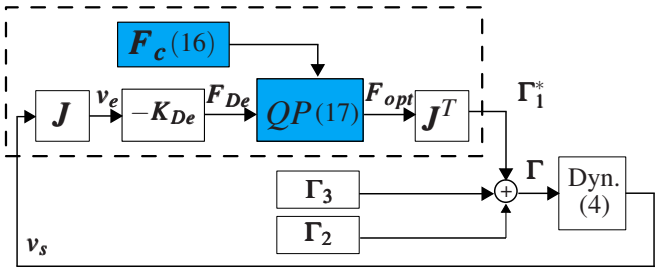

Fig. 3: Block diagram of the controller augmented with QP. The main differences compared to Fig. 2 are highlighted in blue. An open source solver like qpOASES [31] may be used for real-time implementation, which has already proven successful in robot control methods focusing on contact force limitations [32].

threshold of the allowable maximum contact wrench $\boldsymbol{F_{max}}$, for the optimized control effort $\boldsymbol{F_{opt}}$.

The second constraint in (19) is considered in order to ensure the convergence of the controller as required in (14). Physically, this implies that the optimized controller will guarantee that the rate of change in energy of the end-effector motion does not increase due to the optimization. Therefore, the structure of the controller can be augmented with the QP optimization and is show in Fig. 3.

V. Validation Results

The validation of the proposed control strategy is performed for a post-grasp scenario in MATLAB/Simulink with an integration time step of 1 ms. A servicer spacecraft with mass $m = 700$ kg and inertia parameters $I_x = 400, I_y = 450, I_z = 400, I_{xy} = I_{xz} = I_{yz} = 0$ kgm^2, equipped with the 7-DoF DLR CAESAR manipulator arm (see [18] for details about the arm), is considered. The mass and inertia parameters of the client are $m = 200$ kg and $I_x = 120, I_y = 100, I_z = 90, I_{xy} = -0.5, I_{xz} = -0.8, I_{yz} = -0.4$ kgm^2, and its initial tumbling velocity is set to $\begin{bmatrix}7.071 & -7.071 & 0\end{bmatrix}^T$ deg/s. The lever arm from the center of mass of the client to its grasping point is 0.5 m. The initial state of the servicer is assumed to be that of the final state at the time of grasping with velocity-matching at the grasp point.

The initial configuration of the manipulator arm is chosen as $\boldsymbol{q} = \begin{bmatrix}-14 & 22 & 21 & 62 & 140 & -24 & -35\end{bmatrix}^T$ deg. The desired final configuration of the arm is an *elbow-up* configuration, $\boldsymbol{q^d} = \begin{bmatrix}0 & 20 & 0 & -45 & 0 & -45 & 0\end{bmatrix}^T$ deg, suitable for further manipulation/servicing tasks. In order to show the effectiveness of the control, a smooth interpolated trajectory from initial to final joint configuration is provided such that the manipulator approaches a kinematic singularity. The gains $\boldsymbol{K_{De}} = 100\boldsymbol{I}_{6\times6}$, $\boldsymbol{K_{Db}} = 500\boldsymbol{I}_{6\times6}$, $\boldsymbol{K_{Dq}} = 100\boldsymbol{I}_{7\times7}$, $\boldsymbol{K_{Pq}} = 500\boldsymbol{I}_{7\times7}$ are used for the controller. The allowable maximum contact force, $\boldsymbol{F_{max}}$, is a settable parameter dictated by mission requirements, which for this simulation has been set to be 2 N for the forces and 2 Nm for the torques to test an extreme case with very small values. The weighting matrix for the optimization is $\boldsymbol{Q} = \text{diag}(1/\boldsymbol{F}_{\boldsymbol{max}_i}^2)$.

The results of the simulation for the nominal controller, i.e. the controller without the QP solver in the loop, designed in (13), are shown in Fig. 4 and Fig. 5. Although the simulation runs for 70 s, Fig. 4 shows the data for the first 20s to better visualize the results. The client's tumbling motion is seen to be entirely damped within 10 s in Fig. 4(a), while the contact wrench in Fig. 4(b) clearly violates the maximum force $\boldsymbol{F_{max}}$.

The base velocity, on the other hand, is seen to increase before getting damped in Fig. 5(a), while the joint errors converge to zero in Fig. 5(b). This shows how the base is activated by the nullspace in order to reconfigure the arm. Notice that, after the client motion has been damped, the nullspace control is still active, yet the contact forces stay close to zero (see time interval 10-20 s in Fig. 4 and Fig. 5).

The measure of kinematic singularity of the arm is computed as $\det(\boldsymbol{J_m}\boldsymbol{J_m}^T)$, where a value equal to zero indicates a singular configuration. As can be seen in Fig. 5 (c), the manipulator arm approaches a singular configuration at 12 s. This does not affect the convergence of the joint task in the nullspace, consistent with the discussion in Sec. III-.3.

The same scenario is considered for the QP-optimized controller constraining the contact forces, and the results are shown in Fig. 6 (data for the first 20 s is shown for better visualization). The client's tumbling motion is seen to be damped within 20 s in Fig. 6(a), while the contact wrench in Fig. 6(b) is strictly maintained below $\boldsymbol{F_{max}}$, as imposed by the constraint given in (18). The slower rate of detumbling in Fig. 6(a) compared to Fig. 4(a) is a consequence of the optimization that limits the maximum contact force.

Fig. 7(a) shows the rate of change of energy of the end-effector motion $\boldsymbol{v_e}^T\boldsymbol{F_{opt}}$, which maintains the strictly decreasing behaviour required by the convergence constraint in (19). For completeness, the convergence of the joint angle errors is shown in Fig. 7(b). As can be seen, these evolve similarly to those in Fig. 5 (b) since the joint task is achieved in the nullspace of the end-effector.

Fig. 8 shows the different stages of configuration of the servicer-client system, for the simulated detumbling strategy, starting from the initial pose to the final pose, while approaching a singular arm configuration at $t = 12$ s.

Further, a robustness analysis for the same detumbling scenario is performed. This considers uncertainties in the client parameters sampled from a uniform distribution with bounds set to, $\pm 20\%$ for mass, $\pm 20\%$ for inertia parameters, and a sphere of radius 0-5 cm for the center of mass. The maximum error between allowable wrench $\boldsymbol{F_{max}}$ and the developed contact wrench, $\boldsymbol{F_c}$, has been calculated. The corresponding results are shown in a scatter plot in Fig. 9 for 30 simulation runs. It is seen that the maximum error along any component of force and torque are $\Delta f = 0.02$ N and $\Delta\tau = 0.01$ Nm, which is below 1% and 0.5% of the maximum threshold. The results confirm the robustness of the controller to uncertainties in the client parameters.

VI. Conclusion

In this paper, we presented a control strategy for the post-grasp motion stabilization of a tumbling non-cooperative client satellite, while considering space mission requirements such as the maximum allowable contact force and reconfiguration of the manipulator. The constraint on contact

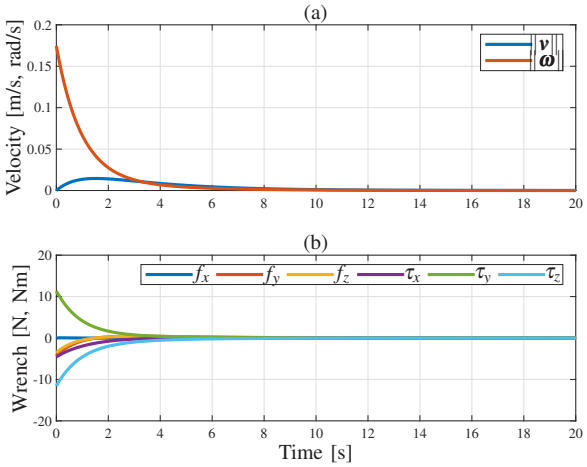

Fig. 4: Detumbling of client using nominal controller in (13). (a) Norm of client velocity (b) Contact Wrench $\boldsymbol{F_c}$.

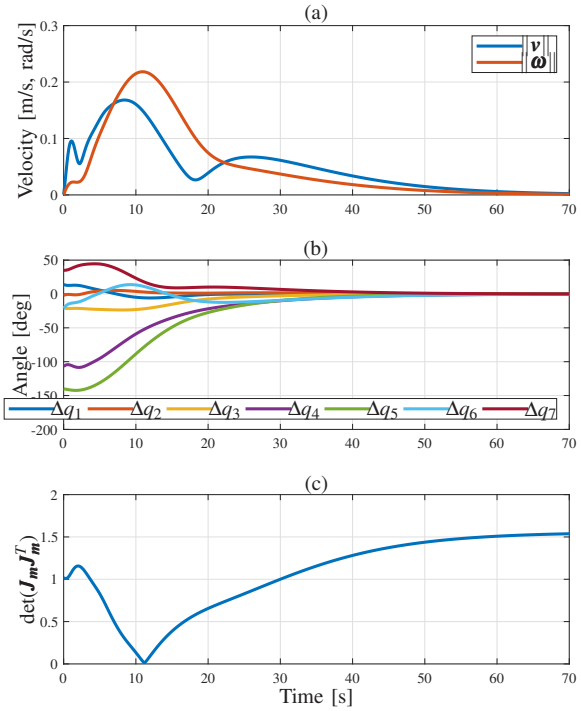

Fig. 5: Reconfiguration of servicer arm using nominal controller in (13). (a) Norm of base velocity (b) Joint angle errors (c) Measure of kinematic singularity of the manipulator arm.

forces was achieved by augmenting the designed controller with a QP algorithm. The reconfiguration of the orbital manipulator was performed entirely in the nullspace of the end-effector using a fully-actuated servicer spacecraft. The effectiveness of the proposed controller was presented for a post-grasp scenario considering a client spinning with an initial velocity of 10 deg/s using a servicer equipped with a 7-DoF manipulator. The convergence of the joints was demonstrated while also approaching a kinematically singular configuration of the manipulator arm. In addition, the proposed controller was shown to be robust to large client parameter uncertainties with the violation of constraints not exceeding 1% and 0.5% of the allowable maximum force and torque. Future work shall consider on-ground experimental validation with discrete actuation of the base.

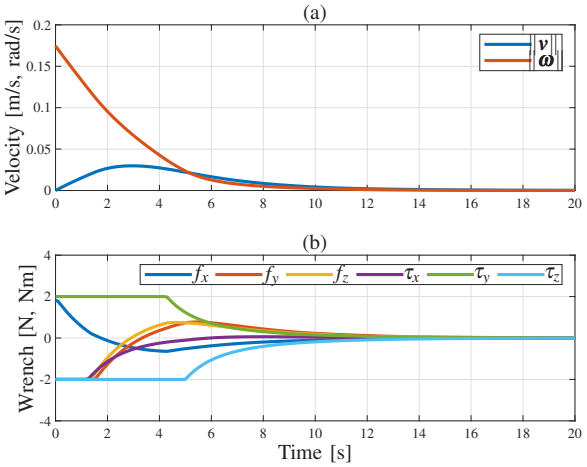

Fig. 6: Detumbling of client using QP-optimized controller. (a) Norm of client velocity (b) Contact Wrench $\boldsymbol{F_c}$.

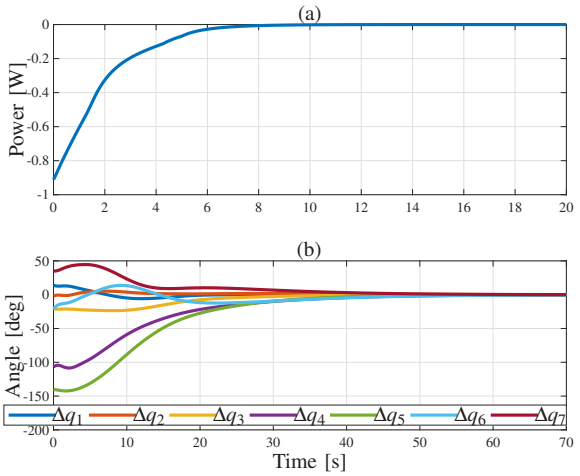

Fig. 7: Results from QP-optimized controller. (a) Energy rate constraint $\boldsymbol{v_e^T F_{opt}}$ (b) Joint angle errors for arm reconfiguration.

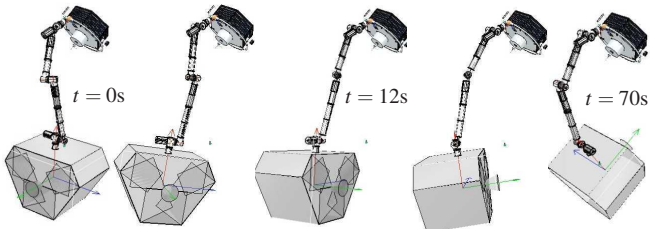

Fig. 8: Stills from an animated motion of the servicer-client system reconfiguring the manipulator arm while stabilizing the client. This can also be seen in the video accompanying the paper.

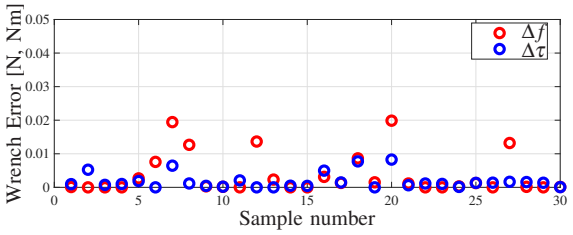

Fig. 9: Maximum deviation of contact wrench calculated for 30 simulations (samples) with client parameter uncertainties.

ACKNOWLEDGMENT

The authors thank Mr. Hrishik Mishra (DLR) for support on the simulation framework.

REFERENCES

[1] A. Flores-Abad, O. Ma, K. Pham, and S. Ulrich, "A review of space robotics technologies for on-orbit servicing," *Progress in Aerospace Sciences*, vol. 68, pp. 1 – 26, 2014.

[2] P. Rank, Q. Mühlbauer, W. Naumann, and K. Landzettel, "The DEOS automation and robotics payload," in *Symp. on Advanced Space Technologies in Robotics and Automation, ASTRA, the Netherlands*, 2011.

[3] P. Colmenarejo, J. Branco, N. Santos, P. Serra, J. Telaar, H. Strauch, A. Giordano, M. De Stefano, C. Ott, M. Rainer, D. Henry, J. Jaworski, E. Papadopoulos, G. Visentin, F. Ankersen, and J. Gil-Fernandez, "Methods and outcomes of the comrade project - design of robust combined control for robotic spacecraft and manipulator in servicing missions: Comparison between hinf and nonlinear lyapunov-based approaches," in *69th International Astronautical Congress*, Sept 2018.

[4] J. Telaar, S. Estable, M. De Stefano, W. Rackl, R. Lampariello, F. Ankersen, and J. Gil Fernandez, "Coupled control of chaser platform and robot arm for the e.deorbit mission," *10th Int. ESA conference on Guidance Navigation and Control Systems (GNC), May 2017*, 2017.

[5] T. Oki, S. Abiko, H. Nakanishi, and K. Yoshida, "Time-optimal detumbling maneuver along an arbitrary arm motion during the capture of a target satellite," in *2011 IEEE/RSJ International Conference on Intelligent Robots and Systems*, 2011, pp. 625–630.

[6] S. Dubowsky and E. Papadopoulos, "The kinematics, dynamics, and control of free-flying and free-floating space robotic systems," *IEEE Transactions on Robotics and Automation*, vol. 9, no. 5, pp. 531–543, 1993.

[7] S. A. A. Moosavian and E. Papadopoulos, "Free-flying robots in space: an overview of dynamics modeling, planning and control," *Robotica*, vol. 25, no. 5, p. 537–547, 2007.

[8] E. Papadopoulos and S. A. A. Moosavian, "Dynamics and control of multi-arm space robots during chase and capture operations," in *Proceedings of IEEE/RSJ International Conference on Intelligent Robots and Systems (IROS'94)*, vol. 3, 1994, pp. 1554–1561 vol.3.

[9] A. M. Giordano, G. Garofalo, and A. Albu-Schaffer, "Momentum dumping for space robots," in *2017 IEEE 56th Annual Conference on Decision and Control (CDC)*, 2017, pp. 5243–5248.

[10] H. Mishra, R. Balachandran, M. De Stefano, and C. Ott, "A compliant partitioned shared control strategy for an orbital robot," *IEEE Robotics and Automation Letters*, vol. 6, no. 4, pp. 7317–7324, 2021.

[11] M. De Stefano, H. Mishra, R. Balachandran, R. Lampariello, C. Ott, and C. Secchi, "Multi-rate tracking control for a space robot on a controlled satellite: A passivity-based strategy," *IEEE Robotics and Automation Letters*, vol. 4, no. 2, pp. 1319–1326, April 2019.

[12] K. Yoshida and H. Nakanishi, "Impedance matching in capturing a satellite by a space robot," in *Proceedings 2003 IEEE/RSJ International Conference on Intelligent Robots and Systems (IROS 2003) (Cat. No.03CH37453)*, vol. 4, 2003, pp. 3059–3064 vol.3.

[13] I. S. Paraskevas and E. G. Papadopoulos, "On the use of the center of percussion for space manipulators during impacts," in *2013 IEEE International Conference on Robotics and Automation*, 2013, pp. 3469–3474.

[14] A. Flores-Abad, M. Nandayapa, and M. A. Garcia-Teran, "Force sensorless impedance control for a space robot to capture a satellite for on-orbit servicing," in *2018 IEEE Aerospace Conference*, 2018, pp. 1–7.

[15] D. Nenchev and K. Yoshida, "Impact analysis and post-impact motion control issues of a free-floating space robot subject to a force impulse," *IEEE Transactions on Robotics and Automation*, vol. 15, no. 3, pp. 548–557, 1999.

[16] K. Yoshida and D. Nenchev, "Space robot impact analysis and satellite-base impulse minimization using reaction null-space," *Proceedings - IEEE International Conference on Robotics and Automation*, vol. 2, pp. 1271–1277, Jan. 1995.

[17] D. Dimitrov and K. Yoshida, "Momentum distribution in a space manipulator for facilitating the post-impact control," in *2004 IEEE/RSJ International Conference on Intelligent Robots and Systems (IROS) (IEEE Cat. No.04CH37566)*, vol. 4, 2004, pp. 3345–3350 vol.4.

[18] A. Beyer, G. Grunwald, M. Heumos, M. Schedl, R. Bayer, W. Bertleff, B. Brunner, R. Burger, J. Butterfaß, R. Gruber, *et al.*, "Caesar: Space robotics technology for assembly, maintenance, and repair," in *Proceedings of the International Astronautical Congress, IAC*, 2018.

[19] F. Aghili, "Optimal control of a space manipulator for detumbling of a target satellite," in *2009 IEEE International Conference on Robotics and Automation*, 2009, pp. 3019–3024.

[20] ——, "Optimal trajectories and robot control for detumbling a non-cooperative satellite," *Journal of Guidance, Control, and Dynamics*, vol. 43, no. 5, pp. 981–988, 2020. [Online]. Available: https://doi.org/10.2514/1.G004758

[21] R. Lampariello, H. Mishra, N. Oumer, P. Schmidt, M. De Stefano, and A. Albu-Schäffer, "Tracking control for the grasping of a tumbling satellite with a free-floating robot," *IEEE Robotics and Automation Letters*, vol. 3, no. 4, pp. 3638–3645, 2018.

[22] R. A. Gangapersaud, G. Liu, and A. H. J. de Ruiter, "Detumbling a non-cooperative space target with model uncertainties using a space manipulator," *Journal of Guidance, Control, and Dynamics*, vol. 42, no. 4, pp. 910–918, 2019. [Online]. Available: https://doi.org/10.2514/1.G003111

[23] L. Shi, X. Xiao, M. Shan, and X. Wang, "Force control of a space robot in on-orbit servicing operations," *Acta Astronautica*, vol. 193, p. 469–482, 2022. [Online]. Available: https://www.sciencedirect.com/science/article/pii/S0094576522000145

[24] S. Abiko, R. Lampariello, and G. Hirzinger, "Impedance control for a free-floating robot in the grasping of a tumbling target with parameter uncertainty," in *2006 IEEE/RSJ International Conference on Intelligent Robots and Systems*, 2006, pp. 1020–1025.

[25] R. M. Murray, Z. Li, and S. S. Sastry, *A mathematical introduction to robotic manipulation*. CRC press, 1994.

[26] C. Ott, *Cartesian impedance control of redundant and flexible-joint robots*. Springer, 2008.

[27] Y. C. Chen and I. Walker, "A consistent null-space based approach to inverse kinematics of redundant robots," in *[1993] Proceedings IEEE International Conference on Robotics and Automation*, 1993, pp. 374–381 vol.3.

[28] O. Khatib, "Inertial properties in robotic manipulation: An object-level framework," *The international journal of robotics research*, vol. 14, no. 1, pp. 19–36, 1995.

[29] X. Wu, C. Ott, , and A. Dietrich, "A comparative experimental study of multi-tasking tracking and interaction control on a torque-controlled humanoid robot," in *2022 American Control Conference (ACC)*, June 2022, accepted.

[30] C. Ott, A. Kugi, and Y. Nakamura, "Resolving the problem of non-integrability of nullspace velocities for compliance control of redundant manipulators by using semi-definite lyapunov functions," in *2008 IEEE International Conference on Robotics and Automation*, 2008, pp. 1999–2004.

[31] J. Ferreau, C. Kirches, A. Potschka, H. Bock, and M. Diehl, "qpOASES: A parametric active-set algorithm for quadratic programming," *Mathematical Programming Computation*, vol. 6, 12 2014.

[32] B. Henze, M. A. Roa, and C. Ott, "Passivity-based whole-body balancing for torque-controlled humanoid robots in multi-contact scenarios," *Int. J. Robotics Res.*, vol. 35, no. 12, pp. 1522–1543, 2016. [Online]. Available: https://doi.org/10.1177/0278364916653815